Frequency-specified EOF analysis and its application to Pacific decadal oscillation

Article *in* Science China Earth Science · December 2016

DOI: 10.1007/s11430-016-0141-x

2 authors:

Tao Lian
Second Institute of Oceanography SOA
21 PUBLICATIONS **226** CITATIONS
SEE PROFILE

Youmin Tang
University of Northern British Columbia
122 PUBLICATIONS **1,219** CITATIONS
SEE PROFILE

SCIENCE CHINA
Earth Sciences

Frequency-specified EOF analysis and its application to Pacific decadal oscillation

LIAN Tao and TANG YouMin

Citation: SCIENCE CHINA Earth Sciences ; doi: 10.1007/s11430-016-0141-x

View online: http://engine.scichina.com/doi/10.1007/s11430-016-0141-x

Published by the Science China Press

SCIENCE CHINA
Earth Sciences

• RESEARCH PAPER •

doi: 10.1007/s11430-016-0141-x

Frequency-specified EOF analysis and its application to Pacific decadal oscillation

LIAN Tao[1*] & TANG YouMin[1,2]

[1] *State Key Lab of Satellite Ocean Environment Dynamics, Second Institute of Oceanography, Hangzhou 310012, China;*
[2] *Environmental Science and Engineering, University of Northern British Columbia, Prince George V2N 4Z9, Canada*

Received October 21, 2016; accepted November 25, 2016; published online December 22, 2016

Abstract A frequency-specified empirical orthogonal function (FSEOF) analysis is proposed in this study. The aim of FSEOF is to specify a prescribed-band of frequency in leading principal components with less information losing at the ends of the data, thus well characterizing the signals of interest. The FSEOF can well capture prescribed variability in leading modes, and has intrinsic merits in resolving frequency-related modes, especially those associated with low frequency oscillations. An application of the FSEOF to the tropical and northern Pacific sea surface temperature shows that this new method can successfully separate Pacific decadal oscillation (PDO) mode from the El Niño-Southern oscillation mode, and clearly detect all regime shifts of PDO in the past century.

Keywords Frequency, EOF, PDO

Citation: Lian T, Tang Y M. 2016. Frequency-specified EOF analysis and its application to Pacific decadal oscillation . Science China Earth Sciences, doi: 10.1007/s11430-016-0141-x

1. Introduction

The empirical orthogonal function (EOF) analysis has been widely used in climate research (e.g. Hannachi, 2004; Lian and Chen, 2012). The leading principal component (PCs) explains the maximum variance whereas the loading (named as eigenvector, e.g., Hannachi, 2004) reflects the corresponding spatial pattern. However, since the EOF analysis is variance based, the associated PCs usually contain a mixture of multiple time scales. It is often of interest to specify a prescribed-band of frequency in the time series.

A traditional way to confine a prescribed-band frequency in leading PCs is to pre-filter data before performing EOF analysis (e.g. Yeh and Kirtman, 2005). In this way, information at the ends of the data is generally discarded or contaminated in a prescribed frequency filter such as the band-pass (or low-pass and high-pass) which is known as the "end effects" (e.g. Zhang and Yuan, 2009) or "edge effects" (e.g. Janecki, 2012). The lost information is often valuable, in particular when the focus is on very low frequency oscillation. An alternative way to decrease information losing is to extend the time series at the beginning and end of data (Minobe, 1999). In this way, arbitrary components may be introduced in the extended samples, which could bias the information of the raw data (e.g., Minobe, 1999).

Recently, the smooth orthogonal decomposition (SOD) method (Chelidze and Zhou, 2006) was introduced into geoscience field (Kuehl et al., 2014). This technique could extract modes with smooth evolution in time, and was expected to be a powerful tool in geoscience. The key of the SOD method is to minimize highest frequency components in the leading PCs while performing EOF analysis. By this, signals with high-frequency components are moved from low order modes to the higher.

In this study, we extend the SOD method to a general case

*Corresponding author (email: liantao@sio.org.cn)

that the leading PCs can contain prescribed frequency components. This is implemented by replacing the minimization of highest frequency components used in SOD, which acts like a high-pass filter, with a prescribed operator that is designed by a specific frequency domain of any interest. We call this as the frequency-specified EOF (FSEOF) analysis. Unlike the traditional way that uses filters or interpolations prior to the EOF analysis, the FSEOF is designed to specify any prescribed-band of frequency in leading modes without requiring pre-filtering or extending the data.

2. Method

The fundamental of the FSEOF method is inherited from the SOD method. That is, to apply simultaneously a frequency-specified filter (a matrix) onto the data while performing the EOF analysis. Given a data matrix $X \in R^{n\times m}$, where m denotes the number of grids and n the number of samples in time, the EOF analysis seeks a linear projection $q=X\varphi$ to maxima the variance of q, namely, $\max_{\varphi}\|X\varphi\|$, where $q \in R^{n\times 1}$ and $\varphi \in R^{m\times 1}$ represent PCs and eigenvectors of matrix X, respectively; $\|.\|$ represents vector mode.

In order to confine the frequency of q in a prescribed-band F_P, we project the raw data X onto a frequency-specified matrix (i.e., filter operator) that is constructed using a set of Fourier basic function with the frequency of F_X, which is beyond F_P. Denoting $D = \{f_i \mid f \in F_X, \text{and} f_i \notin F_P\}$ as the frequency-specified matrix which is constructed using the Fourier basic function with the frequency out of interested, we can design a filtered data $V=D^{\mathrm{T}}X$ which weights the frequencies beyond F_P (Details of the frequency-specified matrix can be found in the Appendix). Thus, the minimization of the variance of V in fact favors the frequencies of F_P, namely, $\min_{\varphi}\|V\varphi\|$, combining $\max_{\varphi}\|X\varphi\|$ and $\min_{\varphi}\|V\varphi\|$, we have the following equation for prescribed-band frequency EOF algorithm:

$$\max_{\varphi}\left\{\lambda(\varphi)=\frac{\|X\varphi\|}{\|V\varphi\|}\right\}=\max_{\varphi}\left\{\lambda(\varphi)=\frac{\varphi^T\Sigma_X\varphi}{\varphi^T\Sigma_V\varphi}\right\}, \quad (1)$$

where Σ_X and Σ_V is the covariance matrix of X and V, respectively. The solution of (1) is very similar to the so-called maximum of Signal-to-Noise Ratio variance, and can be solved by Rayleigh Quotient theorem (e.g. Tang et al., 2008), namely the solution φ is the eigenvector of the below equation (e.g., Chelidze and Zhou, 2006):

$$\Sigma_X\varphi_i=\lambda_i\Sigma_V\varphi_i, i=1,2,..,m. \quad (2)$$

After getting φ, the eigenvectors of (2), we can calculate the corresponding temporal vectors (frequency-specified PCs) by $q=X\varphi$ which explain the maximum variances of raw data at the range of frequencies of F_P. It is worth noting that vector φ_i is not the spatial pattern that corresponds with the derived PCs, because it is not the solution of $\max_{\varphi}\|X\varphi\|$,, but solution of eq. (1). As seen from eq. (2), both the spatial vectors φ and PCs are not orthogonal unless Σ_V is an identical matrix. Therefore, after obtaining the frequency-specified PCs, we regress the data matrix X on q to get the corresponding spatial patterns. This kind of EOF method is called as the frequency-specified EOF (FSEOF) analysis.

It's clear that the fundamental difference between the FSEOF method and the SOD method resides in the frequency-specified matrix. In the SOD method, the frequency-specified matrix is constructed in the way only the highest frequency is used and therefore only the variation with the highest frequency can be removed. On the other hand, the FSEOF method can let one to remove variations with any uninterested frequency by designing the frequency-specified matrix. If the frequency-specified matrix is constructed using Fourier basic function with the highest frequency alone, then the FSEOF method is degenerated as the SOD method. Also noted is the frequency-specified matrix used here is based on the Fourier basic function. One can also use other filtering method to generate the frequency-specified matrix. However, the performance of the FSEOF is not sensitive to the method used to generate the frequency-specified matrix (not shown).

3. A synthetic experiment of FSEOF

A synthetic experiment which is very similar to that used in Chelidze and Zhou (2006) is constructed to show the capability of the FSEOF analysis in confining a prescribed-band of frequency in PCs with less information losing at the ends of data. The data matrix X has eight grids $X=[T_1, T_2, ..., T_8]$, where $T_i=\sin(it)$, $t\in[0, 2\pi]$. As such, X contains a set of periodic oscillations with frequency varying from 1 to 8. The frequency-specified band is set in the range of [2, 3]. Three EOF analyses were performed in this experiment. The first one is to apply the traditional EOF analysis to the raw data. The second one is to apply the traditional EOF to the filtered data that was obtained using a band-pass butter-worth 1-order digital filter (e.g. Shaman, 2014). The last one is using the FSEOF analysis as described above.

The Figure 1a–d shows the first three PCs and their frequency power spectrums while using the traditional EOF analysis to the raw data. None of PCs shows periodic oscillation and their power spectrums are not confined to a signal frequency channel. If the data is pre-filtered, the specified-band frequencies can be captured by the PC1 and PC2. However, their power spectrums are rather weak and flat (Figure 1e–h). Further, the prescribed-band frequencies are also found in PC3, which explain the 26.82% of total variance. This is unexpected since only two grids in the raw data matrix have the specified-band frequencies, which im- plies that the specified-band frequencies should have significant weights in two leading PCs (PC1 and PC2) only.

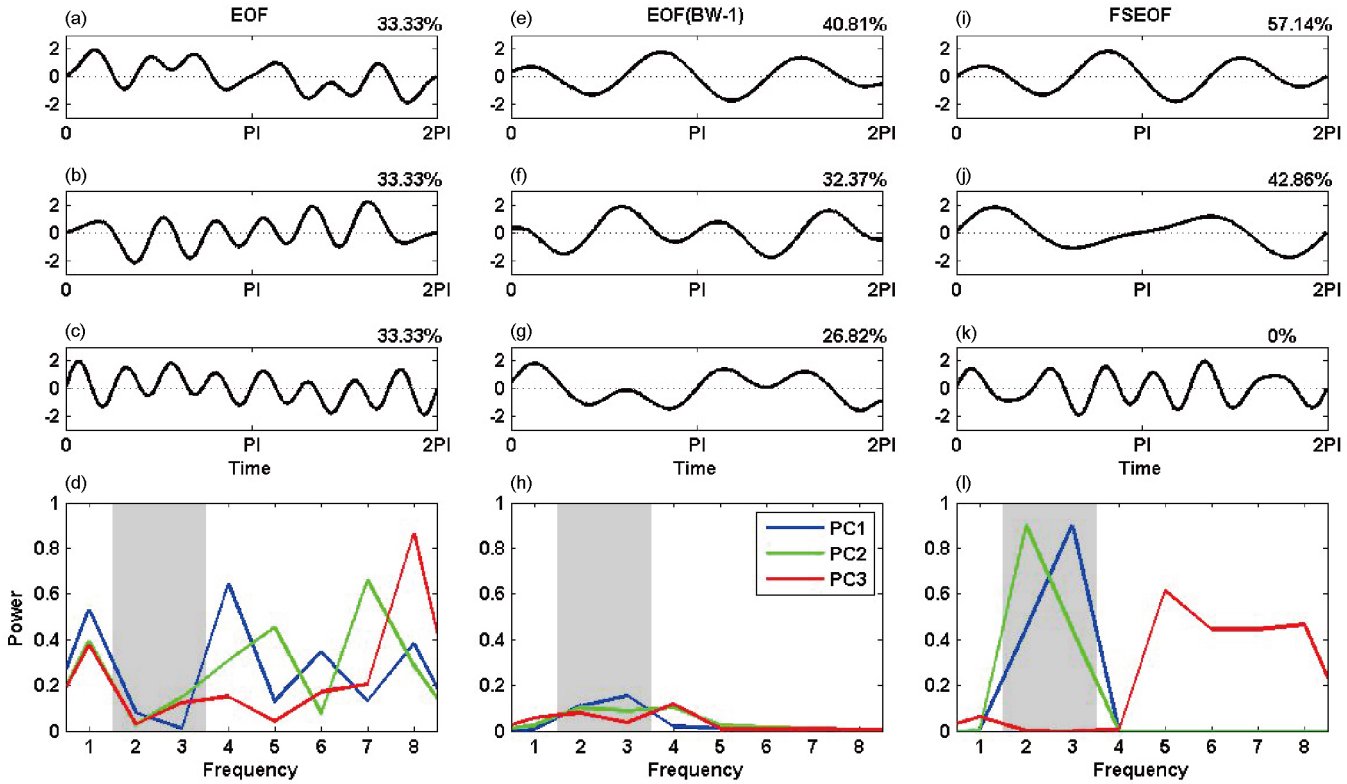

Figure 1 Leading three PCs using the EOF analysis ((a)–(c)), EOF analysis with data pre-filtered by 1-order butter-worth filter ((e)–(g)) and the FSEOF analysis with un-filtered data ((i)–(k)). (d), (h) and (l) are the spectral power of PCs by each method. Grey bar denotes the frequency-specified band. Percentage at right-top of (a), (e) and (i) denotes the explained variance.

Thus, the traditional EOF analysis cannot confine specified-band frequencies in PCs without biasing information.

Shown in Figure 1i–l are the results from the FSEOF. As can be seen, the FSEOF can successfully confine the specified-band frequencies in the PC1 and PC2, with a highly resolved power spectrum at the corresponding frequency band. As expected, the first two modes explain all of the total variances and the higher mode has zero of total variance**.** In experiments with other frequency-specified band ranges (e.g. [3, 4] and [4, 5]), the FSEOF shows the similar merits (not shown).

As we have noted, there is a spurious leaking of variance to higher mode in the pre-filtered EOF (Figure 1e–h). One possible reason is because the digital filter used here is not adequate. In this experiment, we used the first-order butter-worth filter. Generally, the higher order of butter-worth filters the better behavior of the filtered data. To investigate the impact of digit filter on EOF, we performed several sensitivity experiments. Figure 2 shows three pre-filtered EOF temporal modes from the 2nd, 3rd, 4th order butter-worth filter, respectively. The leaking can be greatly reduced through increasing the filter order, as indicated by a progressive decrease of the variance explained by PC3 and the increase of power spectrum of PC1 and PC2. However, on the other hand, higher order digital filters sacrifice more information at the ends of data. In our experiment, the values on each grid are designed to be evolved to zeros at the ends. This characteristic is totally contaminated in the pre-filtered case shown in Figure 2. For example, the last point of the first PC crossing the *x*-axis (i.e. zero value) has a rather distance to the data end, and the distance increases with the increase of the digital order. This un-realistic behavior is mostly due to the "end effects" induced by the filter. Apparently, the FSEOF alleviates greatly the "end effects", as indicated by the value of zero, as in the raw data, approaching at the data end in both PC1 and PC2.

4. An application to PDO study

In this session, we apply the FSEOF analysis to extract the Pacific decadal oscillation (PDO) mode (Zhang et al., 1997). PDO mode is also named as interdecadal Pacific Oscillation in some literature (e.g. Meehl et al., 2009) as its period spans from 15 to 70 years (Minobe, 1997, 1999), and has broad impacts globally (Zhang and Zhou, 2015). The monthly SST data used here is ERSST v3b (Smith et al., 2008) from 1900 to 2010. PDO is defined as the first EOF mode of monthly SST data in Pacific basin north of 20°N (Mantua et al., 1997; Mantua and Hare, 2002). For comparison, we also extracted PDO mode using the traditional EOF applied to the raw data and the pre-filtered data, and using the SOD method applied

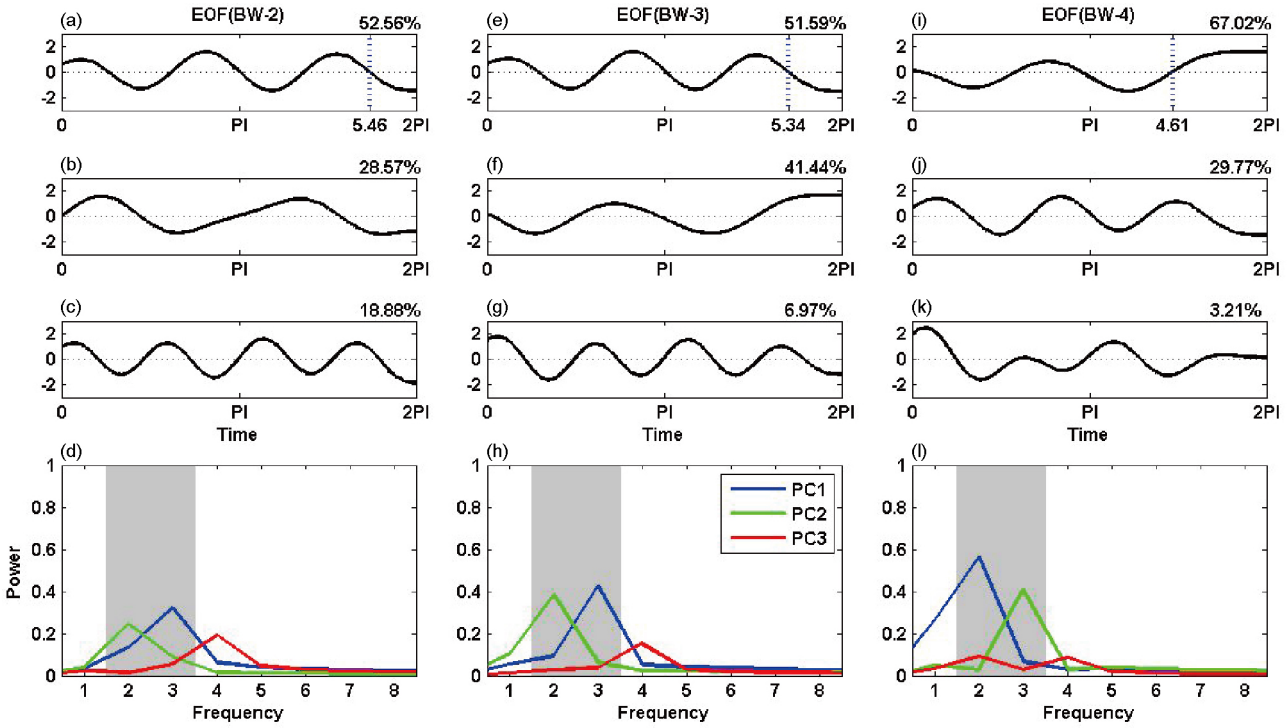

Figure 2 Leading three PCs using the EOF analysis with data pre-filtered by 2-order ((a)–(c)), 3-order ((e)–(g)) and 4-order ((i)–(k)) butter-worth filter. (d), (h) and (l) are spectral power of PCs. Grey bar denotes the frequency-specified band. Percentage at right-top of (a), (e) and (i) denotes the explained variance. The blue dotted line in (a), (e) and (i) denotes the last point where the first PC crossing the *x*-axis.

to the raw data. The annual cycle and the global averaged long-term trend are removed prior to EOF analysis, as in previous studies (e.g., Mantua et al., 1997; Mantua and Hare, 2002).

Figure 3a is the PDO pattern from the traditional EOF applying to the raw data. It is characterized by a dipole structure with one strong pole in the northern central Pacific and the other weak pole around California coastline. The period of PDO varies from biannual to pentadecadal time scale, with the peak around 50 years (Figure 3c). However, the leading PC also displays significant interannual variability in the PDO mode, as shown in Figure 3b and 3c. This is because the PDO pattern is very close to the projection of El Niño-Southern Oscillation (ENSO), a strong interannual oscillation in tropical Pacific, in the northern Pacific (Zhang et al., 1997).

Figure 3d and 3e are the first spatial pattern and the corresponding PC from the EOF of the pre-filtered data, to which a second order band-pass (15–70 years) butter-worth filter was applied. The power spectrum of the first PC is shown in Figure 3f. As can be seen, the major variability has now been well confined in the decadal and interdecadal time scales. Compare to Figure 3a, the spatial pattern in Figure 3d is quite different, with the anomaly center moving southward and eastward. It is different from the classic PDO pattern described in literature (e.g., Mantua et al., 1997). The first PC exhibits an unrealistic anomaly in the early 20th century, which is not shown in the running mean of the PDO index (Figure 3b). The unrealistic feature is apparently associated with the 'end effects' of the filtered data. In addition, there is un-expected regime shift around 1960s in the PC1 (e.g. England et al., 2014). Sensitivity experiments using different orders of filter and periods obtained similar conclusions. It indicates that these unrealistic features of the PDO mode shown in Figure 3d–f are not due to inappropriate choice of filter.

Figure 3g–i are the results from the SOD method. The spatial pattern of the first mode is more like a basin mode. The dominant variation in the first PC is at the centurial time scale, with the peak around 90 years. It's clear that the first mode from the SOD pattern does not represent a decadal oscillation, even though its spatial pattern is close to PDO.

Figure 3j–l are the results from the FSEOF method, with a specified frequency band of 15–70 years. The FSEOF analysis reproduced the classic PDO features on its spatial pattern and the leading PC, including the anomalies distribution in space and phase of regime shifts in time. Compared to Figure 3c and i, the variances explained by the first FSEOF mode is well confined in decadal to interdecadal time scale as expected (Figure 3l). The PC1 in Figure 3k is similar to PC1 in Figure 3b, even at the ends of data period, suggesting that the "end effects" is greatly alleviated by the FSEOF method. Overall, the FSEOF gives a better description of PDO mode at decadal to interdecadal time scale compared with the classic definition of PDO mode.

It has been well recognized that the signal of PDO can be

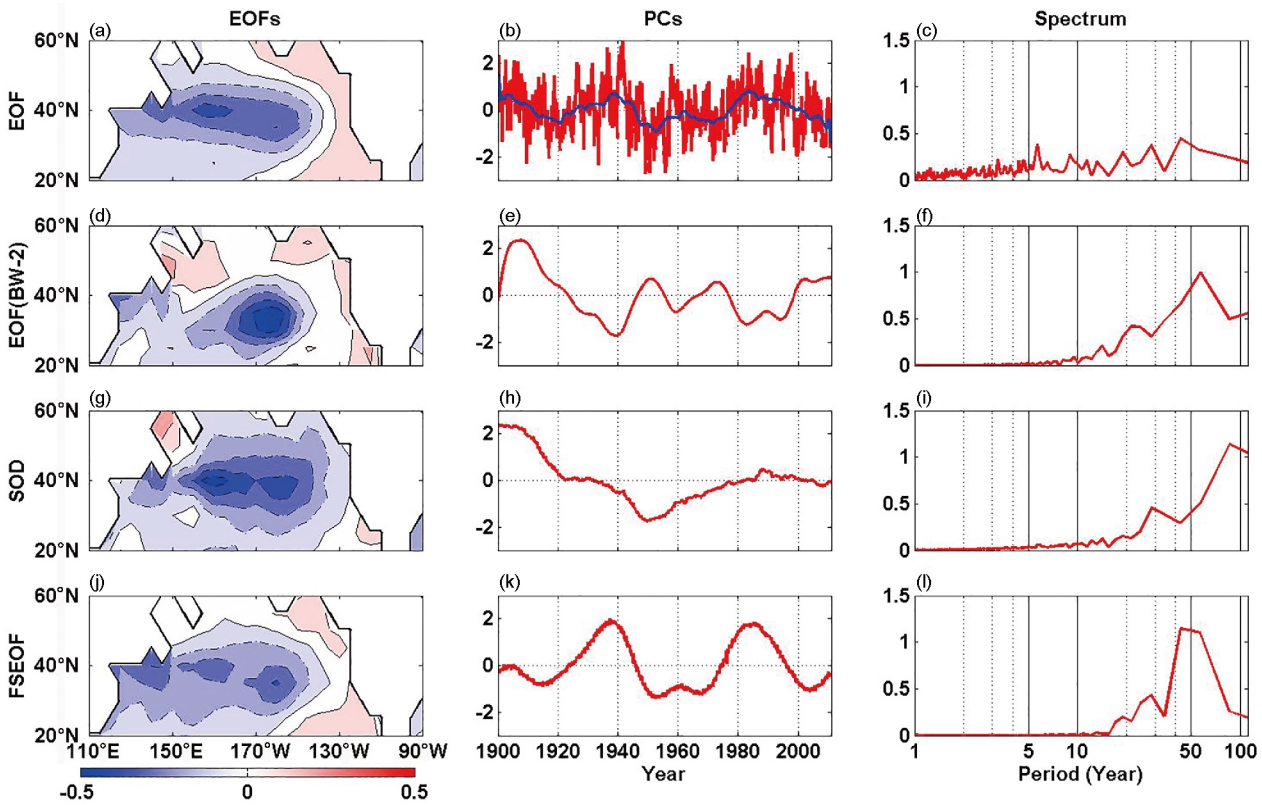

Figure 3 The spatial pattern, PC and the power spectrum of the first mode in northern Pacific deriving by the EOF analysis ((a) to (c)), by the EOF analysis with data pre-filtered by 2-order butter-worth filter ((d) to (f)), by the SOD analysis ((g) to (i)), and the FSEOF analysis ((j) to (l)). The blue line in (b) is the 10-years smoothing. The standard deviation of the smoothed PC is multiplied to (a) in case to uniform all spatial patterns in the same range.

also found in the tropical Pacific region (Zhang et al., 1997; Mantua and Hare, 2002; Deser et al., 2010). However, if the data used for EOF analysis covers both tropical and the northern Pacific, the leading mode of the unfiltered data show the maximum spectrum at interannual scale (Figure 4c). The spatial pattern is more like an ENSO structure with the maximum variance in the tropics (Figure 4a). The decadal to interdecadal variability is mainly characterized in the second and third modes. But the temporal evolution, including the phase of regime shifts, is not correctly presented in these higher modes (not shown) due to the fact that the higher EOF modes can lead to some spurious features (Lian and Chen, 2012). An EOF analysis applied to pre-filtered data can address the decadal signals, as shown in Figure 4f. However, as we have shown above, such a strategy will result in "end effects" in the beginning of data and unrealistic phase shift around 1960s. It is also noted that the tropics contains less decadal or longer time scale variability than subtropical regions, but it still impacts on the spatial structure of decadal mode as represented by the eigenvector (Figure 4d) by pre-filtering process of the data.

Figure 4g–i are the results from the SOD method. The spatial pattern of the first mode is quite different from a PDO-like pattern. The variation is mainly confined in the North Pacific, with the maximum anomaly center in the northwest Pacific. From the variation of the leading PC, it's clear that this first mode reflects the long-term trend of SST in the interested region (Wu et al., 2012). It's worth noting that only the global averaged trend is removed prior to our analysis. At each grid, the local long-term trend is retained. While a PDO-like mode is found as the 3rd mode by the SOD analysis in this case (not shown), its explained variance is much smaller than that of the first two leading modes.

The first leading mode derived by the FSEOF analysis is shown in Figure 4j, with its PC1 and power spectrum shown in Figure 4k and l. Apparently, the leading mode well characterizes the PDO features, in both space and in time. The dipole pattern of the PDO mode and all regime shifts are well reproduced. This example clearly demonstrates the advantage of the FSEOF analysis in extracting the signals of interest that may be even relatively weak in the data.

5. Concluding remarks

One of main issues of the traditional EOF analysis is that its leading PCs often mixes the signals of multiple time scales, making it difficult to characterize the modes of interest. A widely used method to address this issue is to apply filters prior to EOF analysis. However, the application of filters can often bias the information at the ends of data, i.e., the problem

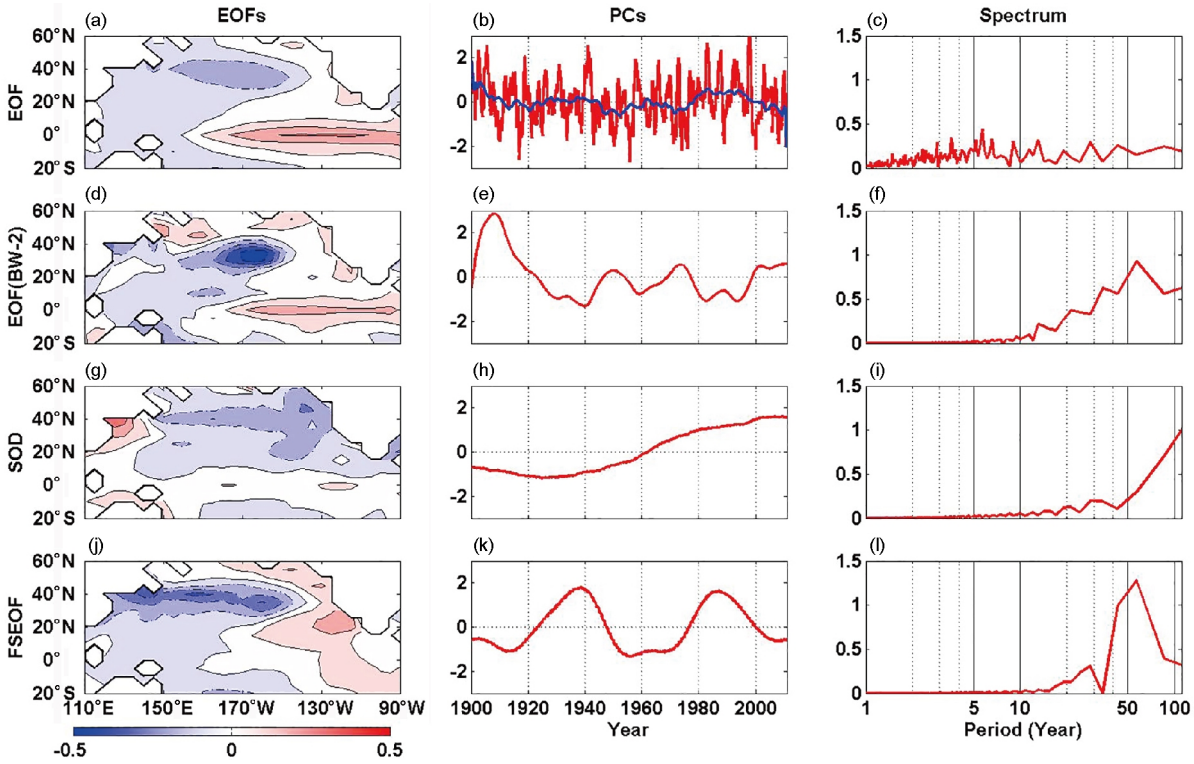

Figure 4 The spatial pattern, PC and the power spectrum of the first mode in tropical and northern Pacific deriving by the EOF analysis ((a)–(c)), by the EOF analysis with data pre-filtered by 2-order butter-worth filter ((d)–(f)), by the SOD analysis ((g)–(i)), and the FSEOF analysis ((j)–(l)). The blue line in (b) is the 10-years smoothing. The standard deviation of the smoothed PC is multiplied to (a) in case to uniform all spatial patterns in the same range.

of "end effects". It is still an open question to extract the modes of interest from the data with multiple time scale variability.

In this study, the FSEOF analysis is proposed to extract frequency-specified band leading modes with less information losing at the data ends. It is found by an idealized experiment that the FSEOF can successfully describe specified-frequency bands in leading PCs as expected. An application of the FSEOF to the Pacific SST data shows the FSEOF analysis can reproduce the classic PDO features on its spatial pattern and the leading PC, with all power spectrums confined within the decadal to interdecadal time scales. The spatial-temporal features of the PDO mode captured by the FSEOF are not shadowed by the stronger ENSO signal even though the data include both ENSO and PDO, due to the strong capability of FSEOF in specifying the signals of interest.

The FSEOF method proposed in this study can be treated as an extension of the SOD method which aims at alleviating high frequency components in the leading PCs (Chelidze and Zhou, 2006). If the operator used in FSEOF contains only the highest frequency band, $\min_{\varphi}\|V\varphi\|$, is similar to a high-pass filter used in SOD and thus the two methods are equivalent. On the other hand if the operator contains all possible frequencies in the data, the Fourier basic function with the frequency out of interest is empty and $\min_{\varphi}\|V\varphi\|$, does not play any role. In this case, the FSEOF is equal to the EOF analysis. Therefore, the FSEOF analysis is flexible and powerful in extracting signals of interests from data.

It is worth noting that the base function used in the FSEOF analysis is the stationary Fourier basic function. If the data is not stationary, the non-stationary wavelet function can be used, instead of the Fourier basic function, to better capture the non-stationary signals. Furthermore, in the current FSEOF algorithm, the Fourier basic function is applied to time series to specify time frequency band. Similarly, this method can be also applied to the eigenvector to specify frequency in space (e.g., one wave signal or two-wave signals). All of these extensions are interesting and under investigation. In particular, as the FSOEF overcomes the ends effects to a large extent, the FSEOF method can be used to construct some real-time climate indices with frequency being in interest. For example, Wheeler and Hendon (2004) introduced an index without time filtering for the purpose of real-time monitoring and prediction of the Madden-Julian Oscillation (MJO). Although no bandpass time filtering is applied, the index is able to strongly discriminate the 30–80 days signal (Ding et al., 2010). Future work will apply the FSEOF method to extract the real-time MJO indices and compare these indices with Wheeler and Hendon's indices. In short, FSEOF provides a new decomposition method of signal, which is expected to have a broad application in the earth sciences.

Acknowledgements *The SST data used here is from the NOAA extended reconstructed SST V.3b (http://www.esrl.noaa.gov/psd/data/gridded/data.ncep.reanalysis.surface.html). This work was supported by the National Basic Research Program (Grant No. 2013CB430302), the National Program on Global Change and Air-Sea Interaction (Grant Nos. GASI-IPOVAI-04 & GASI-IPOVAI-06), the National Natural Science Foundation of China (Grant Nos. 41506025 & 41530961), the Project of State Key Laboratory of Satellite Ocean Environment Dynamics, Second Institute of Oceanography (Grant No. SOEDZZ1504), and the project of Second Institute of Oceanography, SOA (Grant No. QNYC201501).*

Appendix

Supposing n is the number of samples in time. The frequency of oscillation we can recognize by this n-record time series spans from $1/n$ to 0.5 (with period spans from 2 to n). We first build up two matrixes A and B:

$$A = \begin{Bmatrix} A_1 \\ A_2 \\ \cdots \\ A_3 \end{Bmatrix}, \tag{A1}$$

$$B = \begin{Bmatrix} B_1 \\ B_2 \\ \cdots \\ B_3 \end{Bmatrix}, \tag{A2}$$

Here, A_i and B_i are $1\times n$ vectors and denote the oscillation with frequency of i/n. In details, $A_i(k) = \sin\left(2\pi\frac{i}{n}k\right)$ and $B_i(k) = \cos\left(2\pi\frac{i}{n}k\right)$, where k spins from 1 to n. m equals to $[n/2]$. [] denotes the integral function.

Supposing the frequency being in interesting (prescribed-band) spans from f_1 to f_2. We remove all A_i and B_i which has frequency falling in the prescribed-band from matrix A and B, respectively. The resulting matrix A_X and B_X are then concatenate together and construct into the frequency-specified matrix $D=\{AX, BX\}$. It's clear that the frequency-specified matrix only contains oscillatory terms with frequency out of the prescribed-band.

References

Chelidze D, Zhou W. 2006. Smooth orthogonal decomposition-based vibration mode identification. J Sound Vibration, 292: 461–473

Deser C, Phillips A S, Alexander M A. 2010. Twentieth century tropical sea surface temperature trends revisited. Geophys Res Lett, 37: L10701

Ding R, Li J, Seo K H. 2010. Predictability of the Madden-Julian oscillation estimated using observational data. Mon Weather Rev, 138: 1004–1013

England M H, McGregor S, Spence P, Meehl G A, Timmermann A, Cai W, Gupta A S, McPhaden M J, Purich A, Santoso A. 2014. Recent intensification of wind-driven circulation in the Pacific and the ongoing warming hiatus. Nat Clim Change, 4: 222–227

Hannachi A. 2004. A primer for EOF analysis of climate data. Department of Meteorology. Reading: University of Reading. 33

Janecki D. 2012. Edge effect elimination in the recursive implementation of Gaussian filters. Precis Eng, 36: 128–136

Kuehl J J, DiMarco S F, Spencer L J, Guinasso Jr. N L. 2014. Application of the smooth orthogonal decomposition to oceanographic data sets. Geophys Res Lett, 41: 3966–3971

Lian T, Chen D. 2012. An evaluation of rotated EOF analysis and its application to tropical Pacific SST variability. J Clim, 25: 5361–5373

Mantua N J, Hare S R, Zhang Y, Wallace J M, Francis R C. 1997. A Pacific interdecadal climate oscillation with Impacts on salmon production. Bull Amer Meteorol Soc, 78: 1069–1079

Mantua N J, Hare S R. 2002. The Pacific decadal oscillation. J Oceanogr, 58: 35–44

Meehl G A, Hu A, Santer B D. 2009. The Mid-1970s climate shift in the Pacific and the relative roles of forced versus inherent decadal variability. J Clim, 22: 780–792

Minobe S. 1997. A 50–70 year climatic oscillation over the North Pacific and North America. Geophys Res Lett, 24: 683–686

Minobe S. 1999. Resonance in bidecadal and pentadecadal climate oscillations over the North Pacific: Role in climatic regime shifts. Geophys Res Lett, 26: 855–858

Shaman J. 2014. The seasonal effects of ENSO on European precipitation: Observational analysis. J Clim, 27: 6423–6438

Smith T M, Reynolds R W, Peterson T C, Lawrimore J. 2008. Improvements to NOAA's historical merged land-ocean surface temperature analysis (1880–2006). J Clim, 21: 2283–2296

Tang Y, Kleeman R, Moore A M. 2008. Comparison of information-based measures of forecast uncertainty in ensemble ENSO prediction. J Clim, 21: 230–247

Wheeler M C, Hendon H H. 2004. An all-season real-time multivariate MJO index: Development of an index for monitoring and prediction. Mon Weather Rev, 132: 1917–1932

Wu L, Cai W, Zhang L, Nakamura H, Timmermann A, Joyce T, McPhaden M J, Alexander M, Qiu B, Visbeck M, Chang P, Giese B. 2012. Enhanced warming over the global subtropical western boundary currents. Nat Clim Change, 2: 161–166

Yeh S W, Kirtman B P. 2005. Pacific decadal variability and decadal ENSO amplitude modulation. Geophys Res Lett, 32: L05703

Zhang H, Yuan Y B. 2009. Approximating spline filter: New approach for gaussian filtering in surface metrology. Graphics and Signal Processing, 1: 9–16

Zhang Y, Wallace J M, Battisti D S. 1997. ENSO-like interdecadal variability: 1900–93. J Clim, 10: 1004–1020

Zhang L X, Zhou T J. 2015. Decadal change of East Asian summer tropospheric temperature meridional gradient around the early 1990s. Sci China Earth Sci, 58: 1609–1622